Supporting Information

Targeting the imperfections at the ZnO/$CsPbI_2Br$ interface for low-temperature carbon-based perovskite solar cells

Xiang Zhang,[‡a] Dan Zhang,[‡a] Tonghui Guo,[a] Junjie Zou,[a] Junjun Jin,[a] Chunqiu Zheng,[c] Yuan Zhou,[a] Zhenkun Zhu,[a] Zhao Hu,[d] Qiang Cao,[a] Sujuan Wu,[c] Jing Zhang,[b] Qidong Tai*[a]

[a] The Institute of Technological Sciences, Wuhan University, Wuhan 430072, P. R. China

[b] Department of Microelectronic Science and Engineering, Ningbo University, Zhejiang 315211, P. R. China

[c] Institute for Advanced Materials, South China Academy of Advanced Optoelectronics, South China Normal University, Guangzhou 510006, P. R. China

[d] School of Material Science & Engineering, Wuhan Institute of Technology, Wuhan 430073, PR China

‡ These authors contributed equally to this work.

* Corresponding authors. E-mail: qdtai@whu.edu.cn

Experimental Section

Material

Indium-doped tin oxide (ITO) glass (sheet resistance: 7-9 Ω sq^{-1}), cesium iodide (CsI, 99.999%), [6,6]-phenyl-C_{61}-butanoic acid methyl ester ($PC_{61}BM$) and Lead (II) bromide ($PbBr_2$, 99.999%) were bought from Advanced Election Technology Co., Ltd.. Lead iodide (PbI_2, 99.99%) was purchased from Xi'an Polymer Light Technology Corp, China. Cesium acetate (CsAc, 99.9% metals basis), cesium trifluoroacetate (CsTFA) and chlorobenzene (CB, 99.9%) were provided by Alfa Aesar. Cesium fluoride (CsF, 99.9% trace metals basis), N,N-Dimethylformamide (DMF, 99.8%) and Dimethyl sulfoxide (DMSO, ≥ 99.9%) were obtained from Sigma-Aldrich. Zinc acetate dihydrate ($Zn(Ac)_2 \cdot 2H_2O$, 99.995%), 2-Methoxyethanol (anhydrous, 99.8%) and ethanolamine (standard for GC, >99.5%) were gotten from Aladdin. Absolute ethanol, isopropyl alcohol (IPA) and acetone were received from Sinopharm. Commercial carbon pastes (MTW-CE-C-003) were purchased from Shanghai Materwin New Materials Co., Ltd.. Unless otherwise specified, all of materials and reagents were used as received without any further purification.

ZnO/doped ZnO Precursor Solution Preparation

Zinc oxide (ZnO) precursor solution was prepared by dissolving 100 mg $Zn(Ac)_2 \cdot 2H_2O$ powder in 1 mL 2-Methoxyethanol and 27.5 μl ethanolamine, and stirred at least 12 h and filtered through a pore 0.22 μm PTFE filter before use. For doped ZnO precursor solution, different amounts of cesium modulators (CsF, CsAc and CsTFA) were added into the prepared ZnO precursor solution.

$PC_{61}BM$ Preparation

$PC_{61}BM$ film was fabricated by spin-coating 20 mg mL^{-1} $PC_{61}BM$ CB solution at 4000 rpm for 30 s in nitrogen (N_2)-filled glovebox.

Device fabrication

ITO glass substrate (1.5 cm ×1.5 cm) was cleaned by sequential ultrasonic treatment in detergent, deionized H_2O, acetone, IPA and absolute ethanol, and then dried with N_2 flow and treated with ultraviolet (UV)-ozone for 15 min. After that, pristine or doped ZnO precursor solution was spin-coated on the ITO glass substrate at 4000 rpm for 40 s, followed by annealing at 150 °C for 30 min in humid air (25 °C, 60-65 % relative humidity (RH)). After cooling down to room temperature, the obtained glass/ITO/electron transport layer (ETL) substrate was immediately transferred into the N_2-filled glovebox. To prepare perovskite film, $CsPbI_2Br$ precursor solution (1.2 M) was prepared by dissolving 1.2 M CsI, 0.6 M $PbBr_2$ and 0.6 M PbI_2 in the DMSO/ DMF mixed solvents (volume ratio = 4 : 6), and stirred at 70 °C until completely

dissolved. Then, it was filtered through a pore 0.22 μm PTFE filter and spin-coated onto the glass/ITO/ETL substrate at 1000 rpm for 5 s and 3000 rpm for 30 s. Afterward, the glass/ITO/ETL/$CsPbI_2Br$ substrate was placed on a hotplate at 40 °C for 3 min and then at 160 °C for 10 min. Finally, commercial carbon paste was doctor-bladed onto the as-prepared $CsPbI_2Br$ film through a shadow mask with the active area of 0.09 cm^2, followed by heating at 120 °C for 20 min to obtain C-IPSCs with a planar structure of glass/ITO/ETL/$CsPbI_2Br$/carbon.

Characterization

Current density-voltage (J-V) curves were recorded on a Keithley 2400 source meter with a scan rate (reverse voltage from 1.5 to 0 V) of 100 m V s^{-1} under an AM 1.5G illumination (100 mW cm^{-2}) from a Newport solar simulator (Oriel So1 3A 94023A, USA, calibrated by an NREL-certified standard silicon solar cell). Conductivity (σ), electron mobility (μ_e), space-charge-limited current (SCLC) model and dark J-V curves were collected by a Keithley 2400 source meter. The dependence of open-circuit voltage (V_{oc}) and short-circuit current density (J_{sc}) on light intensity (P_{light}) was based on the J-V curves under different illuminations, which were modulated by a series of neutral density filters. External quantum efficiency (EQE) measurement was conducted on a quantum efficiency (QE) system (Enlitech, QE-R666) equipped with 75 W xenon lamp in DC mode. X-ray photoelectron spectroscopy (XPS) was characterized by an X-ray photoelectron spectrometer (Thermo Scientific K-Alpha+, USA) using an Al Ka (*hv* = 1486.6 eV) X-ray excitation source. The C 1s line at 284.6 eV was used to correct all XPS spectra. Ultraviolet photoelectron spectroscopy (UPS) was measured using an ESCALAB Xi+ system (Thermo Fisher, USA) with a He I (*hv* = 21.22 eV) emission line at a base pressure of 5×10^{-8} Torr. X-ray diffraction (XRD) and depth-dependent grazing incident X-ray diffraction (GIXRD) patterns were analyzed by an X-ray diffractometer (Bruker D8 Advance, Germany) with an Cu Kα (λ = 1.5406 Å) radiation source under operating conditions of 40 kV and 40 mA. Fourier-transform infrared (FTIR) spectroscopy was collected using a Nicolet 5700 FTIR spectrometer (Thermo Scientific, USA) with an ATR-diamond. Surface morphology, cross-sectional structure and and energy-dispersive X-ray spectroscopy (EDS) mapping image were obtained by a field-emission scanning electron microscopy (SEM) (Zeiss SIGMA, Germany). Atomic force microscopy (AFM) and Kelvin probe force microscopy (KPFM) images for ETLs were observed by an atomic force microscope (SPM-9700HT, Shimadzu, Japan). Contact angle was measured via an optical video contact angle instrument (Dataphysics OCA 20, Germany) and analyzed with its software. UV-visible (UV-vis) absorption and transmittance spectra were carried out on the UV-vis near-infrared spectrophotometer (Shimadzu UV-2600i, Japan). Steady-state photoluminescence (PL) and

time-resolved PL (TRPL) decay spectra were checked by a fluorescence lifetime spectrometer (Fluo Time 300, Germany) operated at 322 nm excitation laser. Transient absorption (TA) spectroscopy was monitored using a high-speed spectrometer (HARRIA-TA, Light Conversion) with a pump excitation wavelength of 532 nm, which was measured from back side of the perovskite film. Electrochemical impedance spectroscopy (EIS) was performed by an electrochemical workstation (Zahner, Germany) under the 10 mW cm^{-2} white LED light, applying a 20 mV AC signal with a frequency range from 1 Hz to 1 MHz. The obtained EIS data were analyzed by the Z-View software (v2.8b, Scribner Associates, USA). Transient photocurrent (TPC) and transient photovoltage (TPV) decay curves were detected on an electrochemical workstation (Zahner, Germany) with a white light LED (80 mW cm^{-2}). Capacitance-voltage (C^{-2}-V) measurements were also tested on an electrochemical workstation (Zahner, Germany). Unless stated otherwise, all of characterizations were carried out in ambient air (25 °C, 20-30% RH).

Calculation

Calculations based on density functional theory (DFT) were conducted on the Gaussian 16 software.[1] The PBE0 functional and mixed basis set (SDD ECP basis set for Cs atom and the 6-311G(d) basis set for other atoms) were adopted for all calculations.[2-4] The DFT-D3 with BJ-damping was applied to correct the weak interaction to improve the calculation accuracy. [5] The IEFPCM implicit solvation model was used to account for the solvation effect.[6]

Figure Section

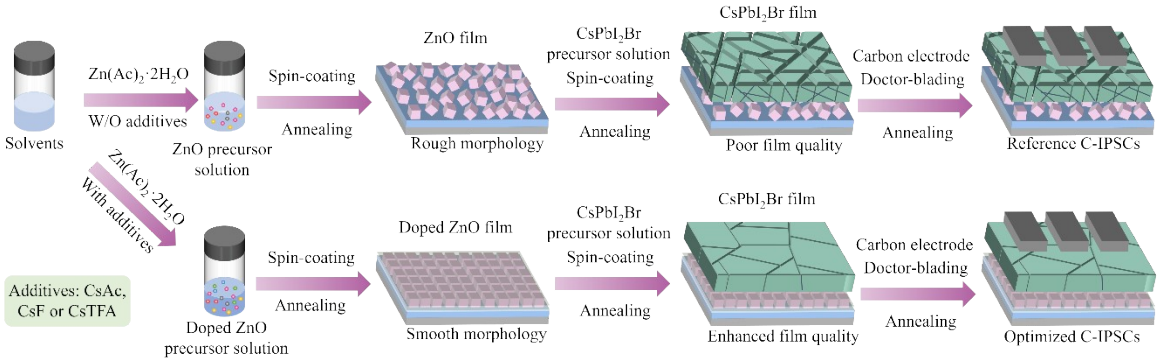

Fig. S1 Schematic diagram for the fabrication process of $CsPbI_2Br$ C-IPSCs.

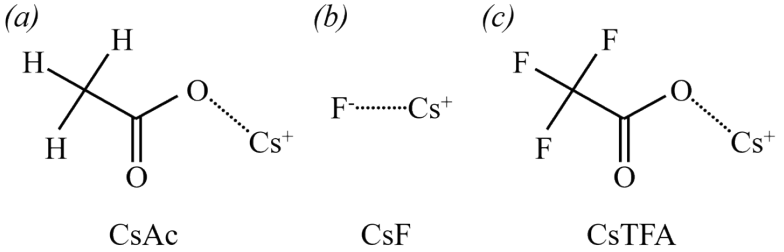

Fig. S2 Molecular structure of (a) CsAc, (b) CsF, and (c) CsTFA.

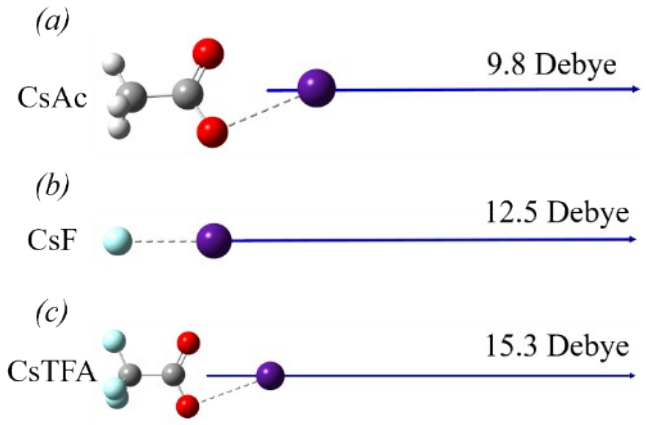

Fig. S3 Dipole moment of (a) CsAc, (b) CsF, and (c) CsTFA.

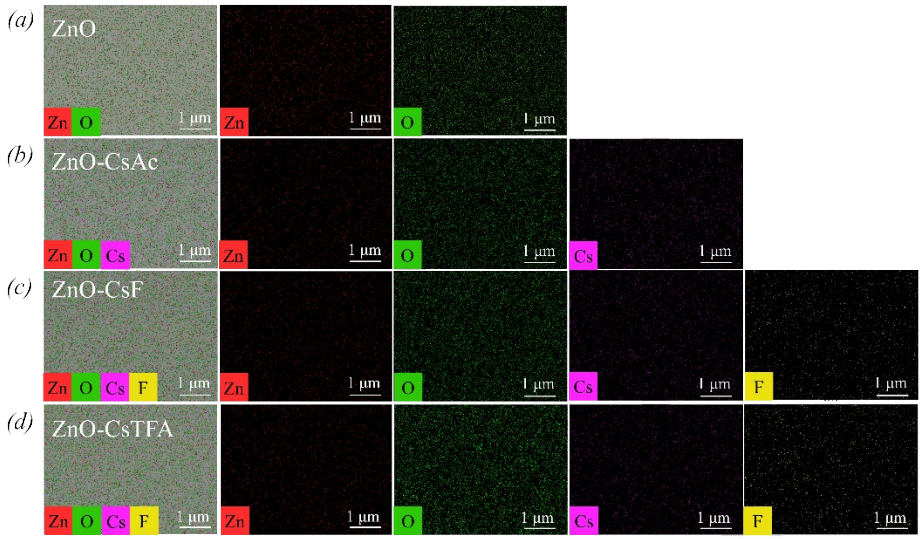

Fig. S4 EDS mapping images of (a) ZnO, (b) ZnO-CsAc, (c) ZnO-CsF, and (d) ZnO-CsTFA ETLs.

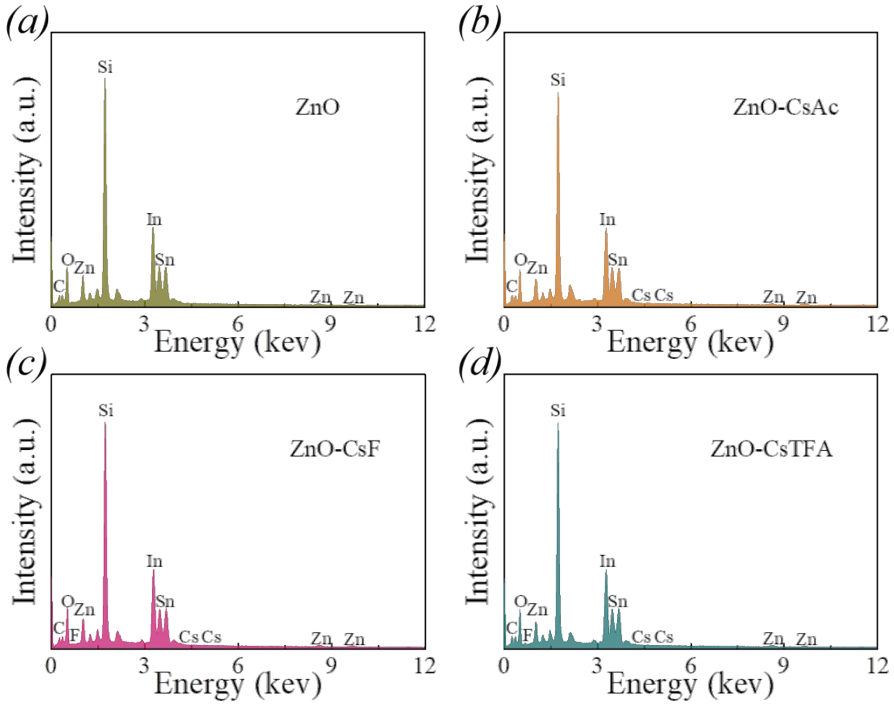

Fig. S5 EDS analysis of (a) ZnO, (b) ZnO-CsAc, (c) ZnO-CsF, and (d) ZnO-CsTFA ETLs.

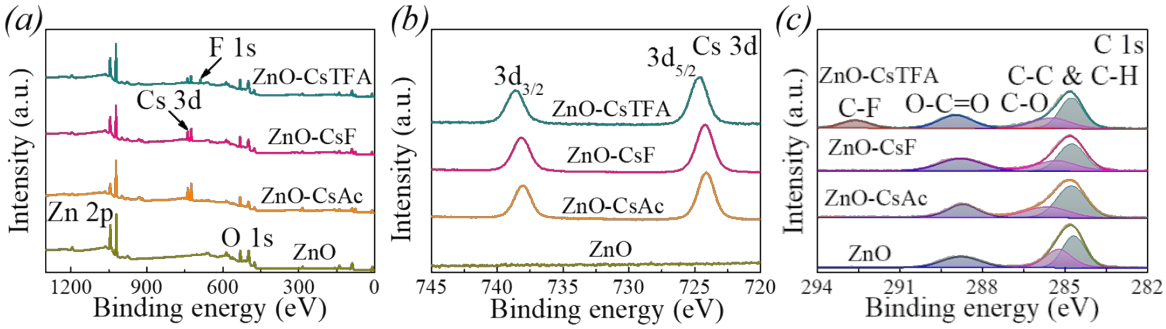

Fig. S6 (a) Full XPS survey spectra. (b) Cs 3d and (c) C 1s XPS spectra of pristine and doped ZnO ETLs.

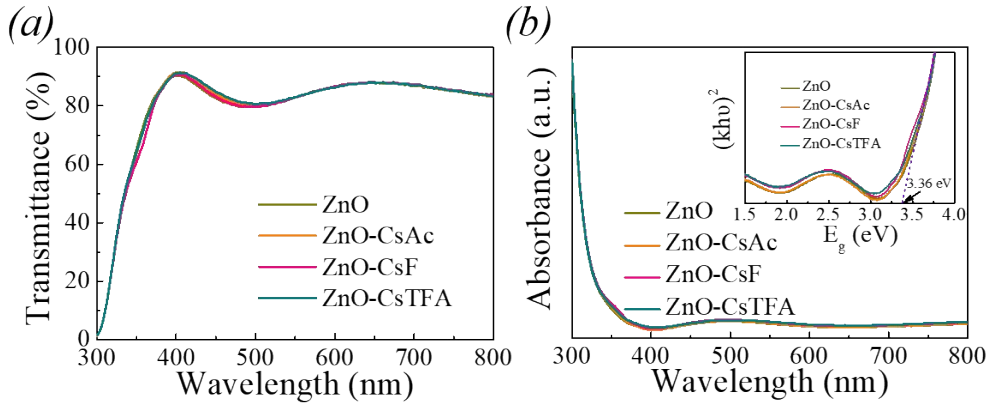

Fig. S7 (a) Transmittance spectra and (b) UV-vis absorption spectra of pristine and doped ZnO ETLs. Inset: corresponding E_g values.

The band gap (E_g) of pristine and doped ZnO ETLs can be calculated by the Tauc plots transformed from the UV-vis absorption spectra via Equation S1:[7]

$$\psi(h\vartheta) = \xi(h\upsilon - E_g)^{1/2} \qquad \text{Equation S1}$$

where ψ, hυ, and ξ are the absorption coefficient, photo energy, and arbitrary constant, respectively.

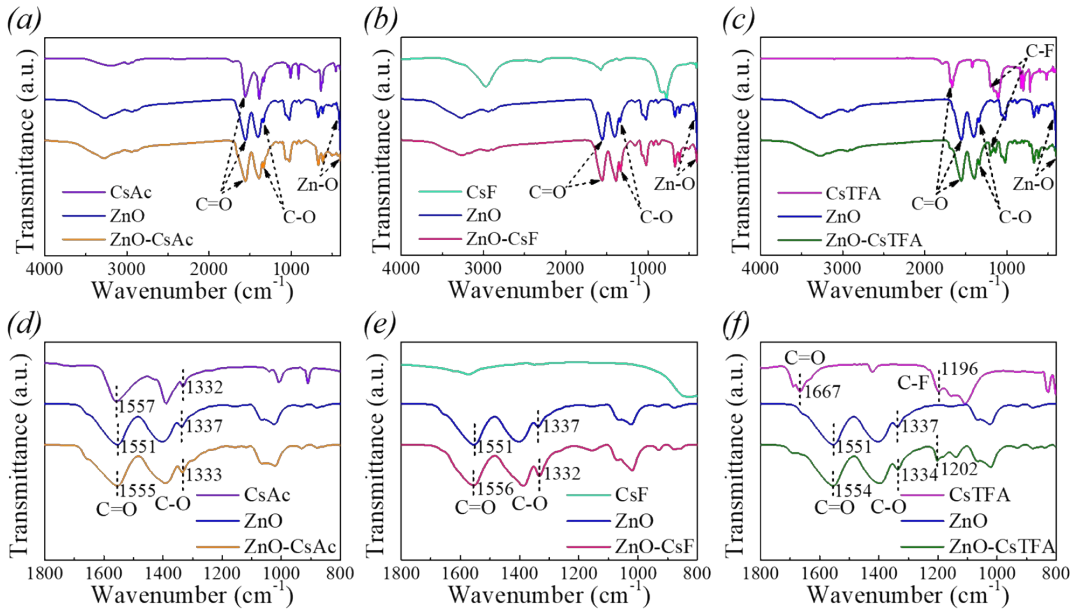

Fig. S8 FTIR spectra of cesium modulators, pristine, and doped ZnO films.

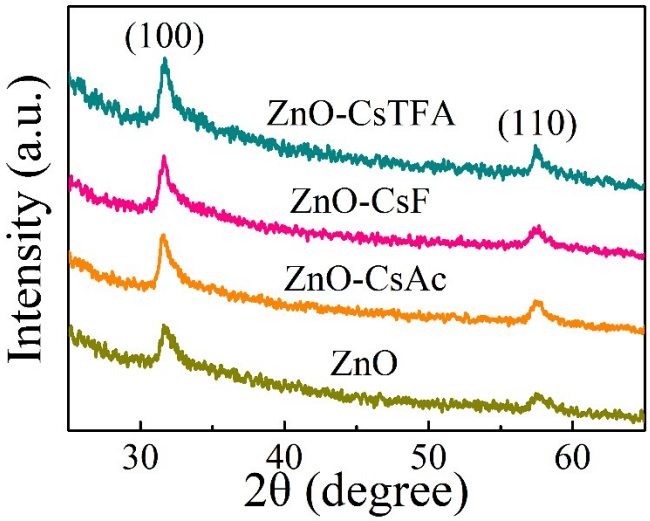

Fig. S9 XRD patterns of pristine and doped ZnO ETLs.

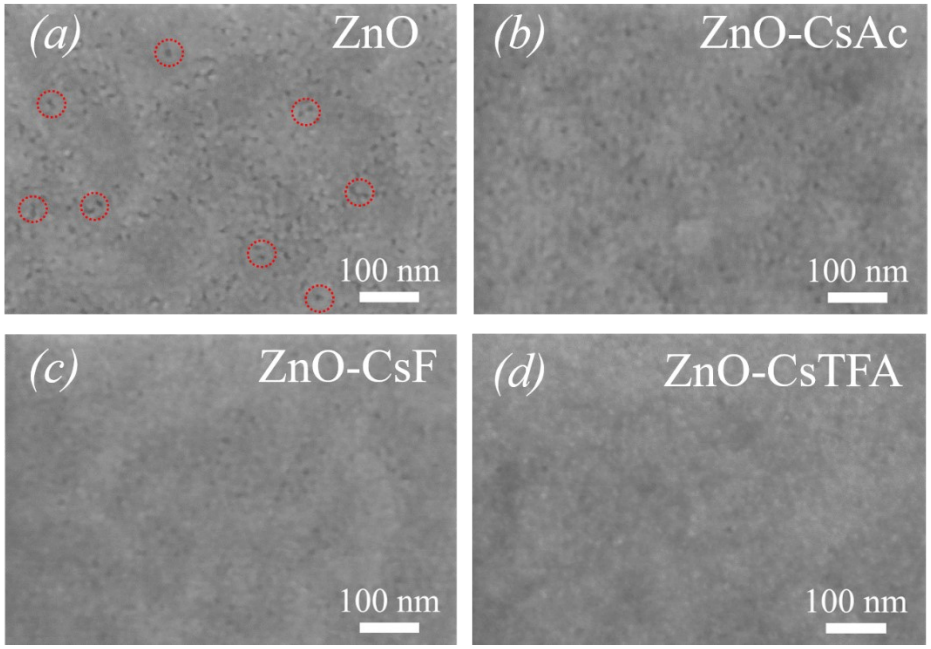

Fig. S10 Top-view SEM images of (a) ZnO, (b) ZnO-CsAc, (c) ZnO-CsF, and (d) ZnO-CsTFA ETLs.

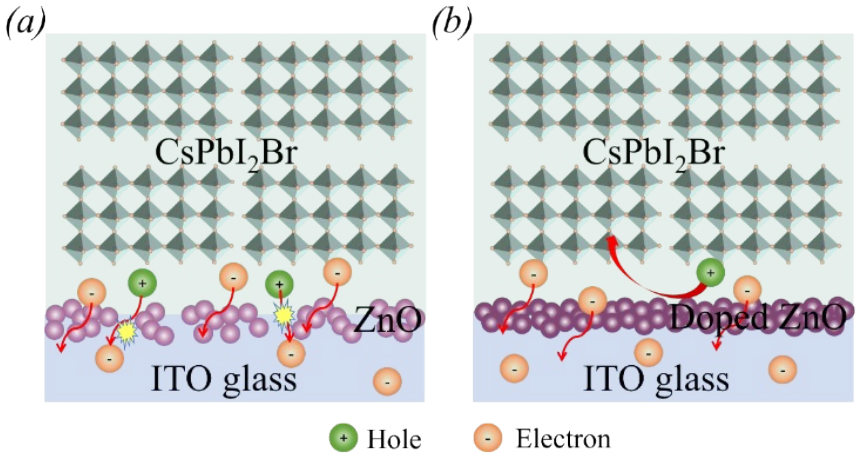

Fig. S11 Schematic illustration of ETL/$CsPbI_2Br$ interfacial contact.

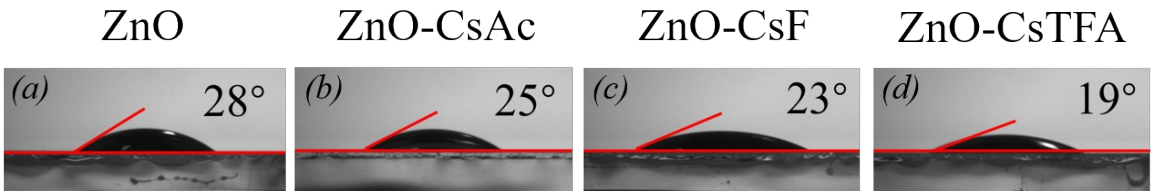

Fig. S12 DMSO/DMF contact angle images of (a) ZnO, (b) ZnO-CsAc, (c) ZnO-CsF, and (d) ZnO-CsTFA ETLs.

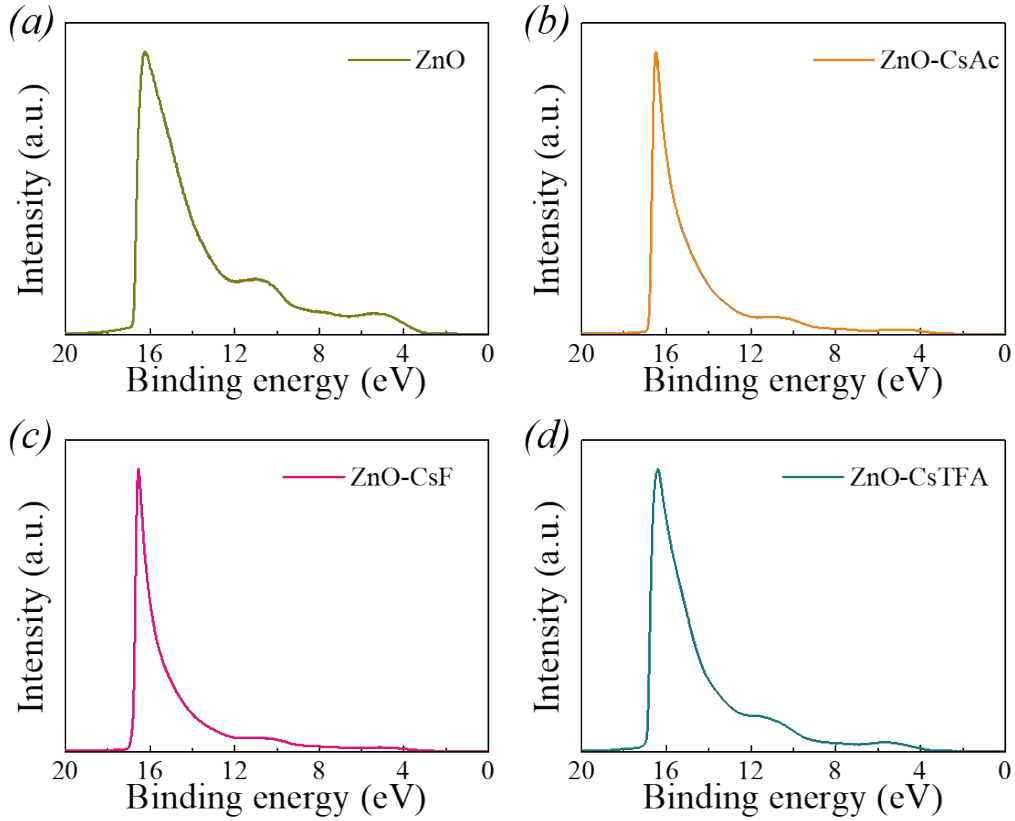

Fig. S13 UPS spectra of (a) ZnO, (b) ZnO-CsAc, (c) ZnO-CsF, and (d) ZnO-CsTFA ETLs.

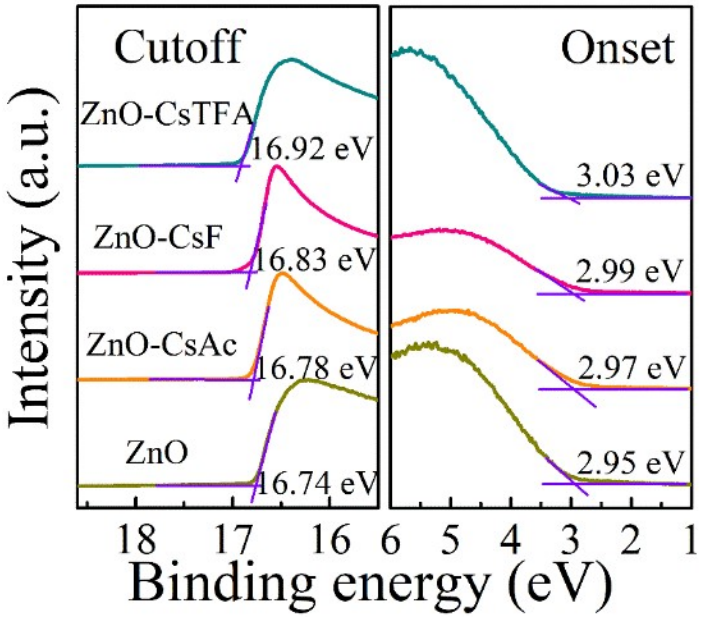

Fig. S14 Detailed parameters derived from the UPS spectra for pristine and ZnO ETLs.

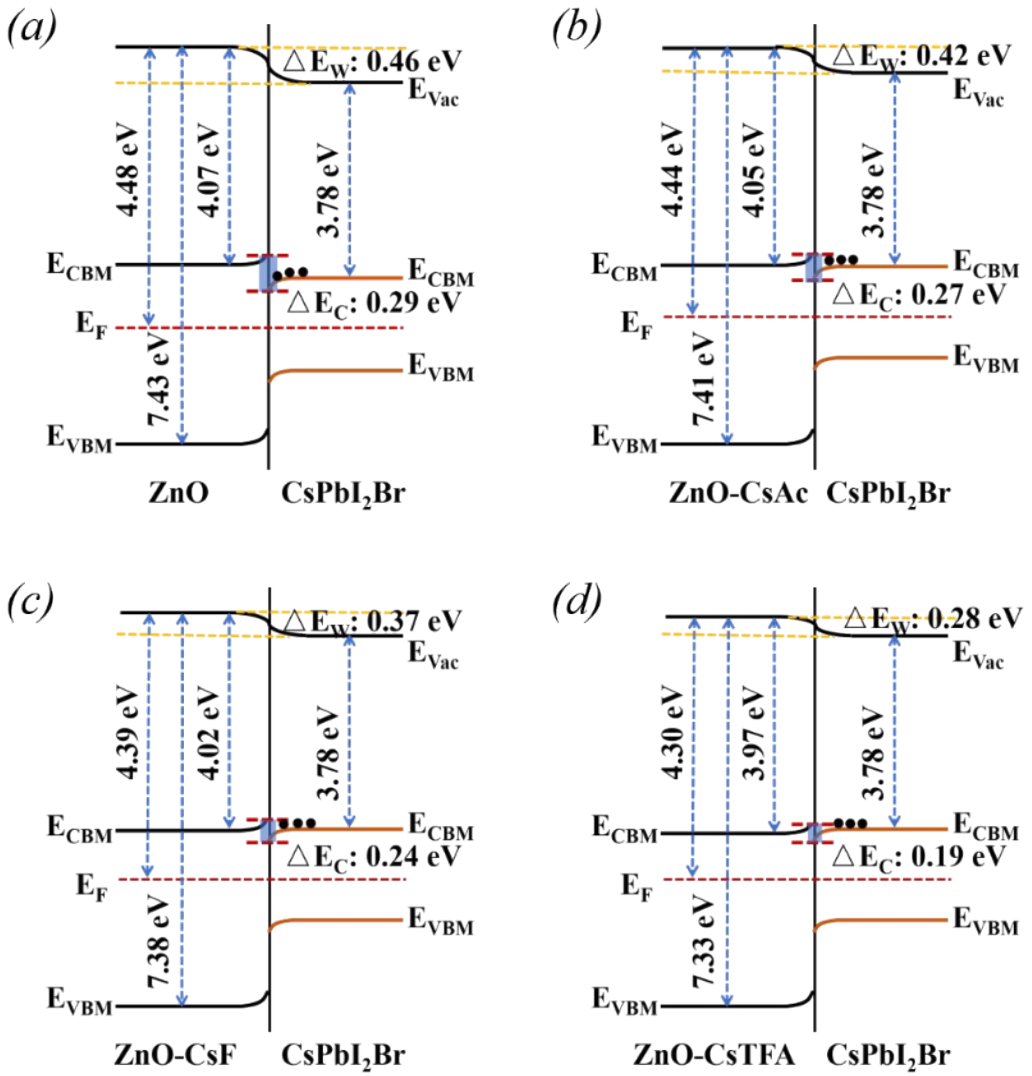

Fig. S15 Energy level diagram for pristine and doped ZnO ETLs compared with $CsPbI_2Br$ films.

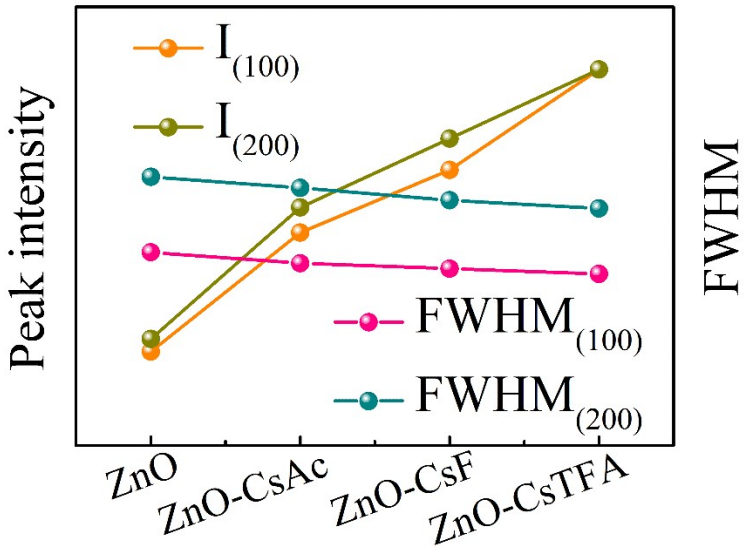

Fig. S16 The relative normalized XRD peak intensity and full-width-at-half-maximum (FWHM) of $CsPbI_2Br$ films on the pristine and doped ZnO ETLs.

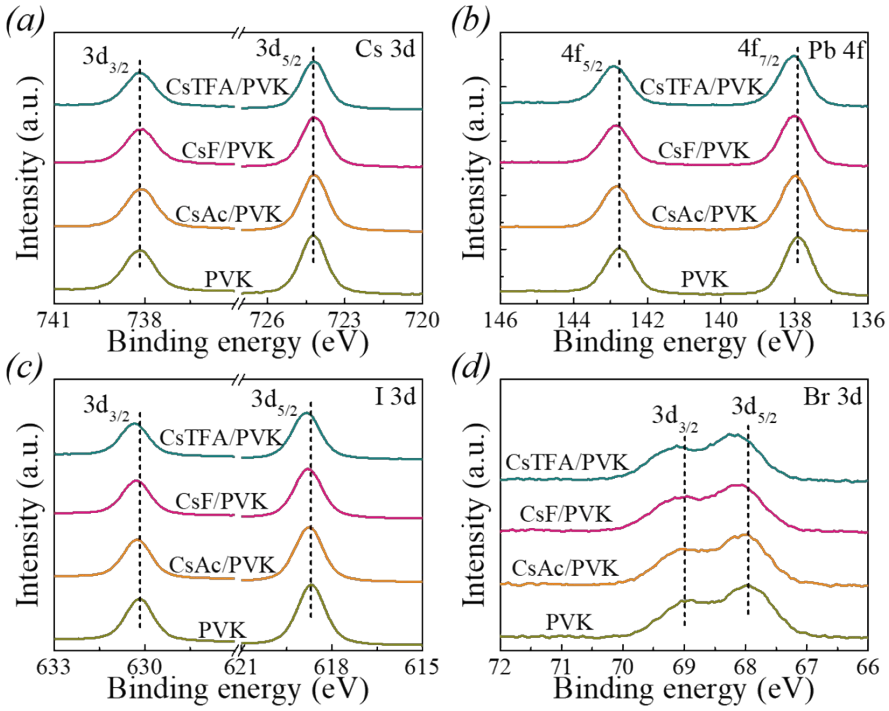

Fig. S17 (a) Cs 3d, (b) Pb 4s, (c) I 3d, and (d) Br 3d XPS spectra of $CsPbI_2Br$ films on the cesium modulator films.

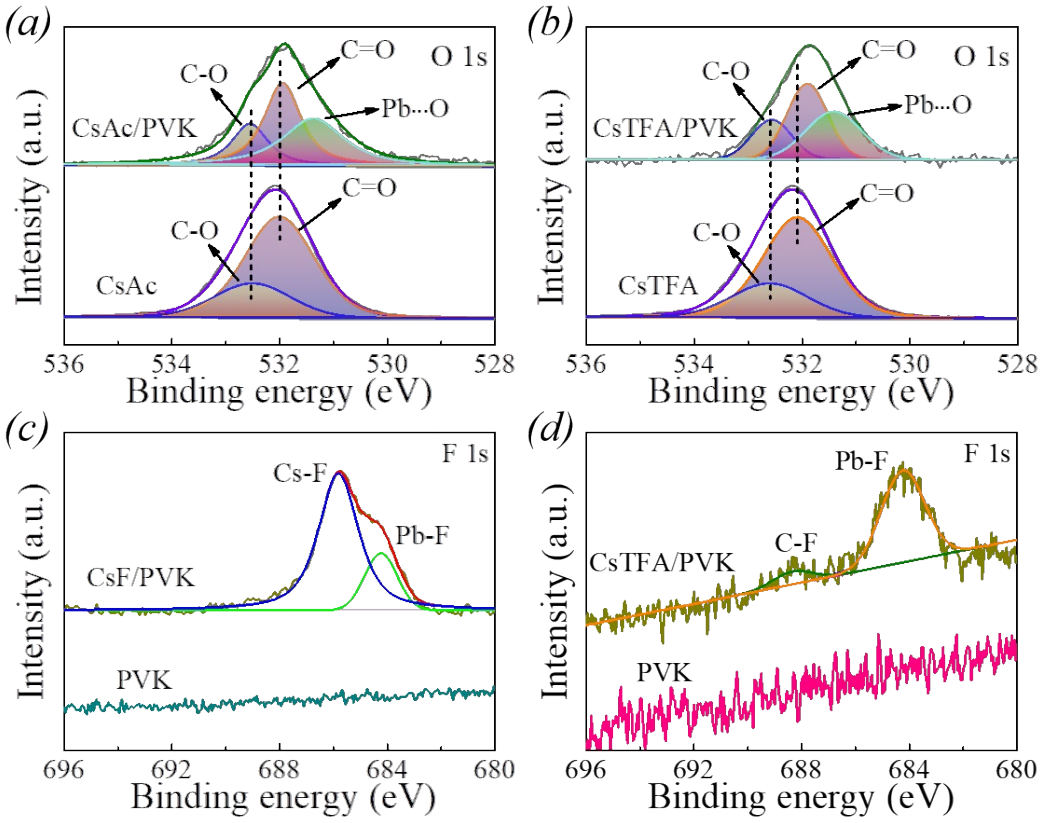

Fig. S18 O 1s XPS spectra of (a) CsAc and CsAc/PVK and (b) CsTFA and CsTFA/PVK. F 1s XPS spectra of (c) PVK and CsF/PVK and (d) PVK and CsTFA/PVK. Note: PVK stands for $CsPbI_2Br$.

To study the the interaction between cesium modulators and perovskite films, we firstly spin-coated 0.5 M cesium modulator precursor solution dissolved in 2-Methoxyethanol/ethanolamine onto the glass substrate, then spin-coated 0.1 M $CsPbI_2Br$ precursor solution onto the cesium modulator films, and finally obtained the samples with a structure of glass/cesium modulators/$CsPbI_2Br$ to measure XPS spectra.

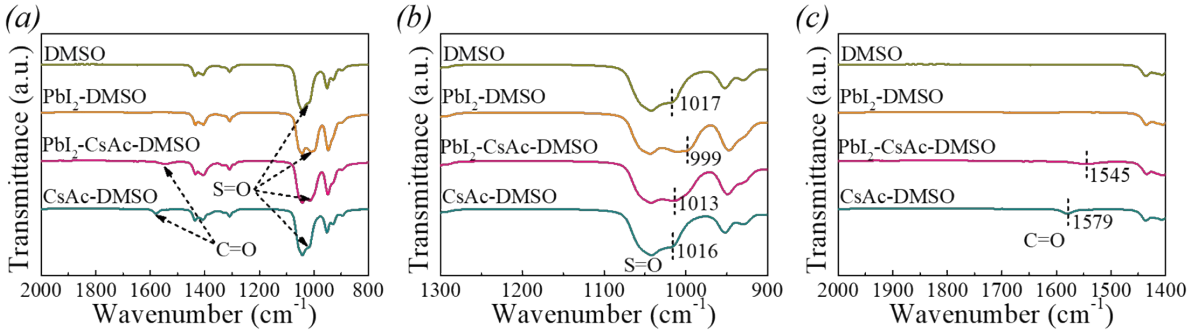

Fig. S19 (a) FTIR spectra and (b-c) fingerprint regions of DMSO (liquid), PbI_2-DMSO (power), PbI_2-CsAc-DMSO (power), and CsAc-DMSO (power). Mixed powders were obtained by adding them in DMSO solvents at 80 °C under stirring for 24 h, followed by removing the solvents by rotary evaporation and drying in a vacuum oven at 65 °C for 48 h.

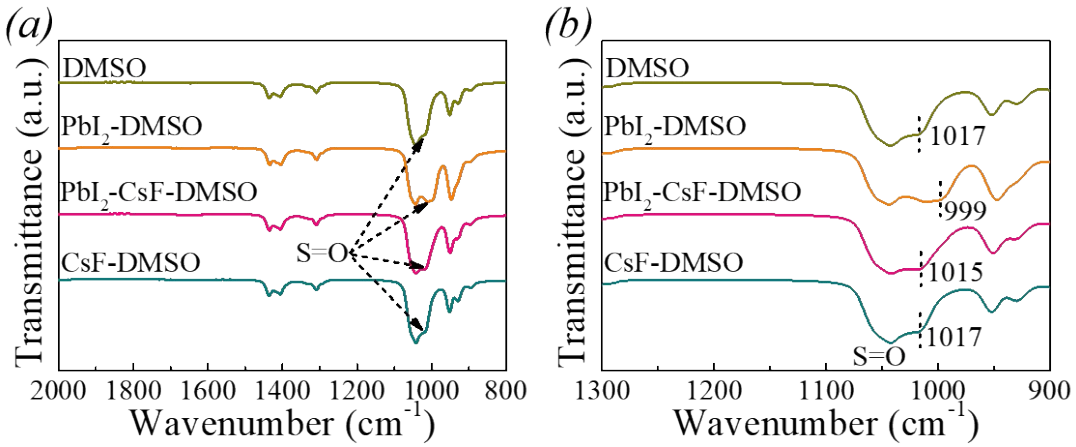

Fig. S20 (a) FTIR spectra and (b) fingerprint regions of DMSO (liquid), PbI_2-DMSO (power), PbI_2-CsF-DMSO (power), and CsF-DMSO (power). Mixed powders were obtained by adding them in DMSO solvents at 80 °C under stirring for 24 h, followed by removing the solvents by rotary evaporation and drying in a vacuum oven at 65 °C for 48 h.

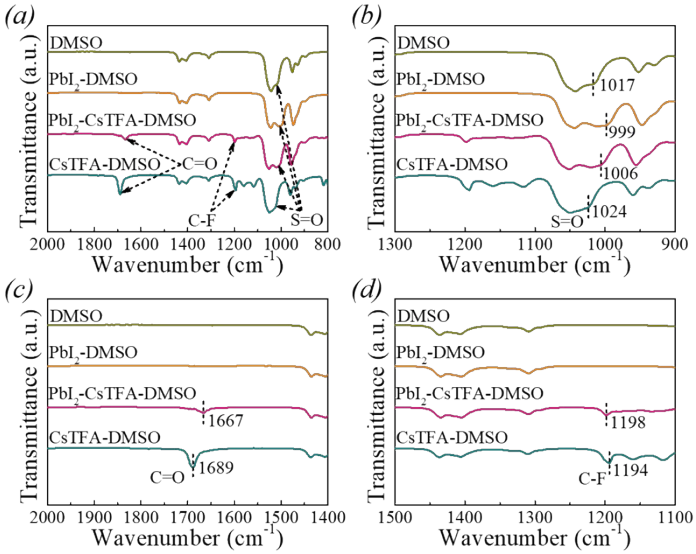

Fig. S21 (a) FTIR spectra and (b-d) fingerprint regions of DMSO (liquid), PbI_2-DMSO (power), PbI_2-CsTFA-DMSO (power), and CsTFA-DMSO (power). Mixed powders were obtained by adding them in DMSO solvents at 80 °C under stirring for 24 h, followed by removing the solvents by rotary evaporation and drying in a vacuum oven at 65 °C for 48 h.

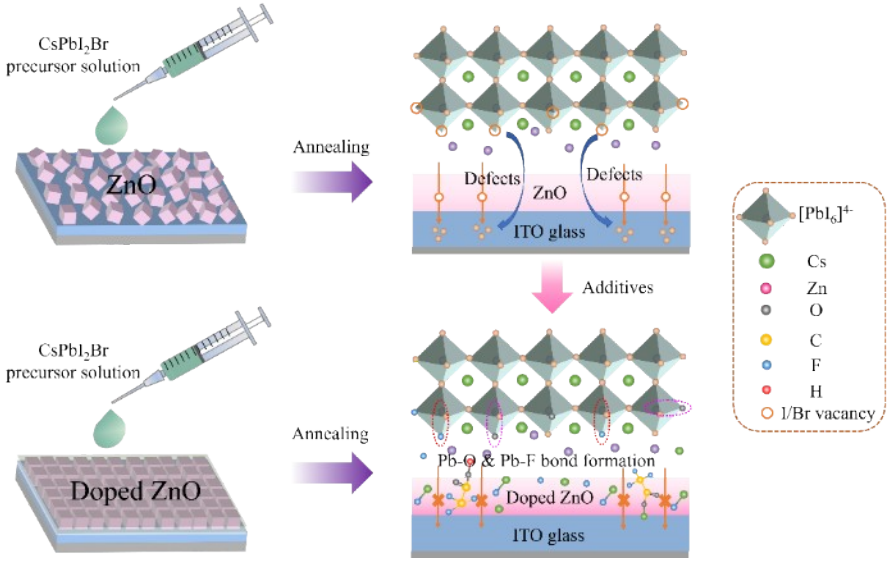

Fig. S22 Schematic illustration of the halide ion migration and passivation mechanism of $CsPbI_2Br$ films on the different ETLs.

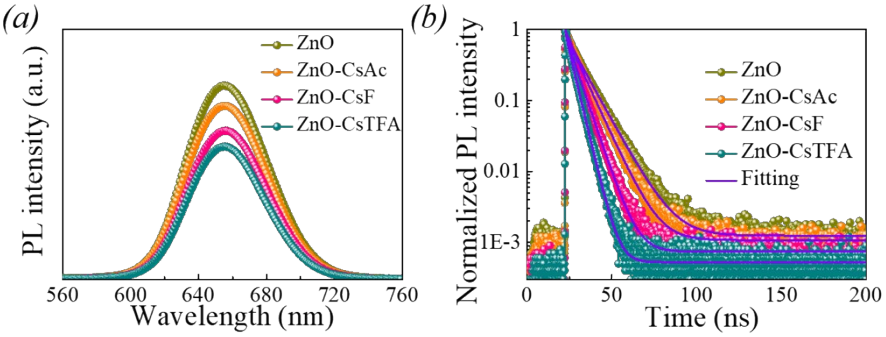

Fig. S23 (a) Steady-state PL and (b) TRPL decay spectra of $CsPbI_2Br$ films on the pristine and doped ZnO ETLs.

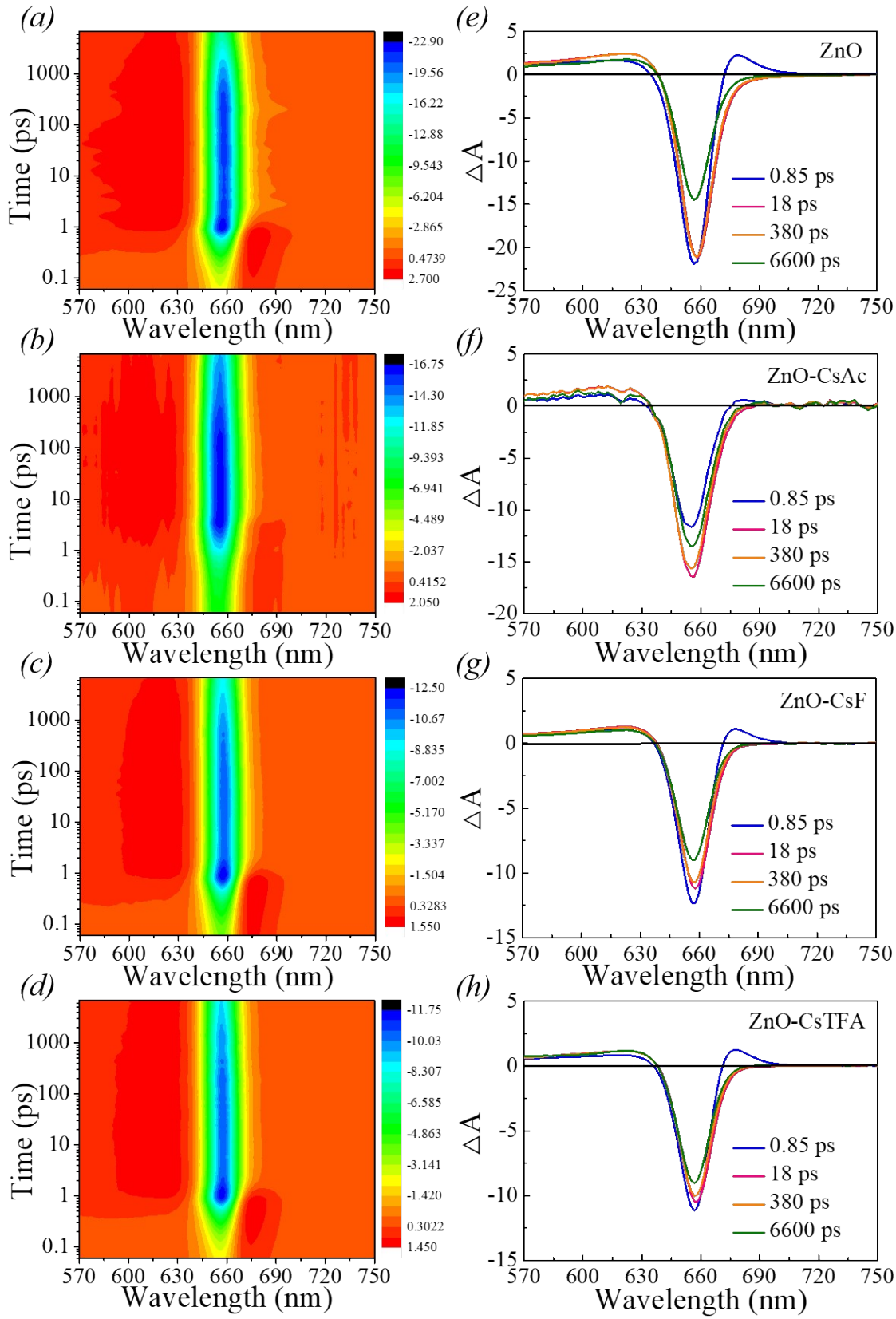

Fig. S24 Two-dimensional pseudocolor plots of TA spectra for $CsPbI_2Br$ films on the (a) ZnO, (b) ZnO-CsAc, (c) ZnO-CsF, and (d) ZnO-CsTFA ETLs. TA spectra of $CsPbI_2Br$ films on the (e) ZnO, (f) ZnO-CsAc, (g) ZnO-CsF, and (h) ZnO-CsTFA ETLs.

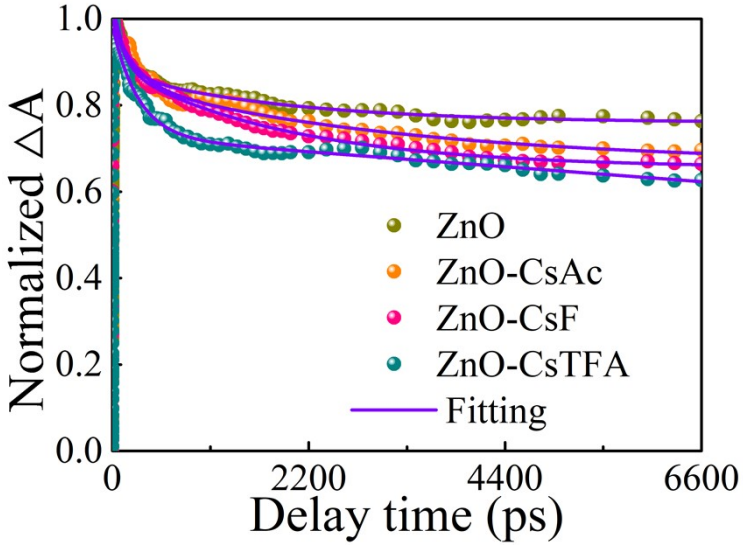

Fig. S25 Normalized kinetic decay traces of PB negative peak for $CsPbI_2Br$ films on the pristine and doped ZnO ETLs.

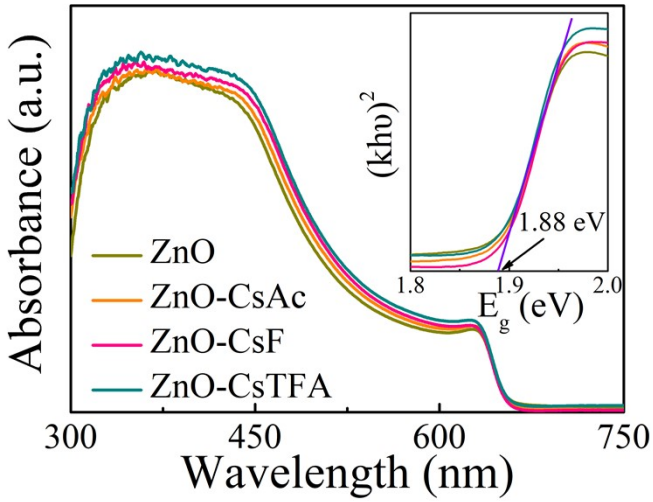

Fig. S26 UV-vis absorption spectra of $CsPbI_2Br$ films on the pristine and doped ZnO ETLs. Inset: corresponding E_g values.

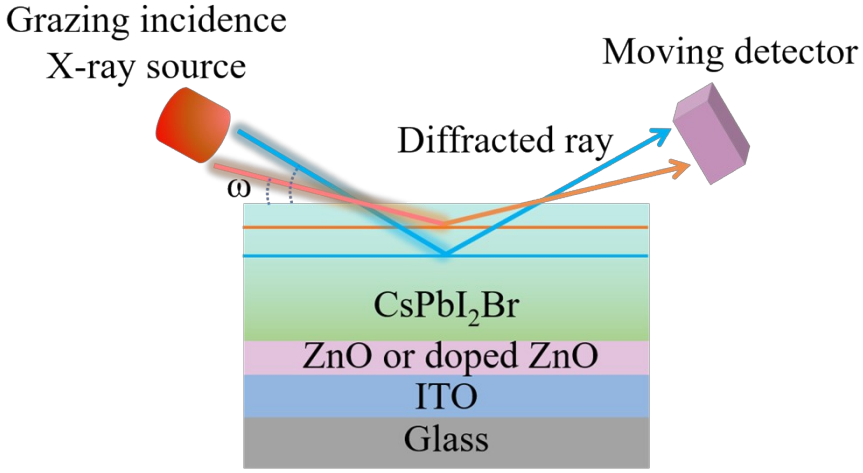

Fig. S27 Schematic diagram of depth-dependent GIXRD measurement.

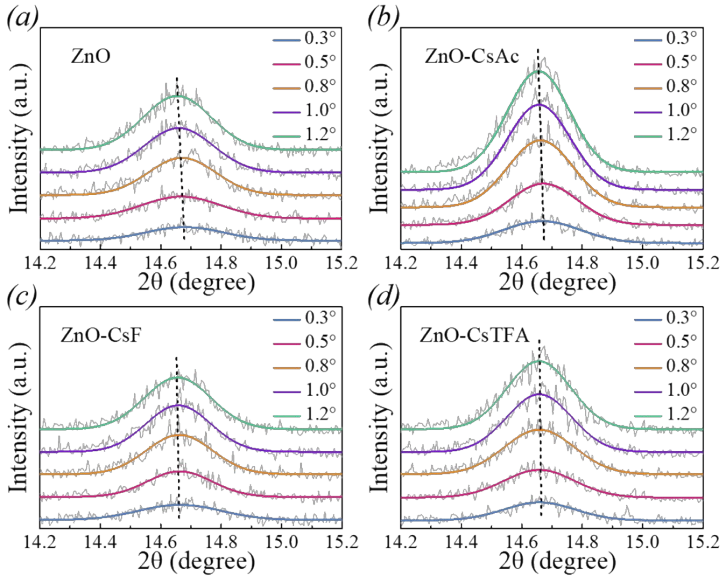

Fig. S28 Depth-dependent GIXRD plots of $CsPbI_2Br$ films on the (a) ZnO, (b) ZnO-CsAc, (c) ZnO-CsF, and (d) ZnO-CsTFA ETLs.

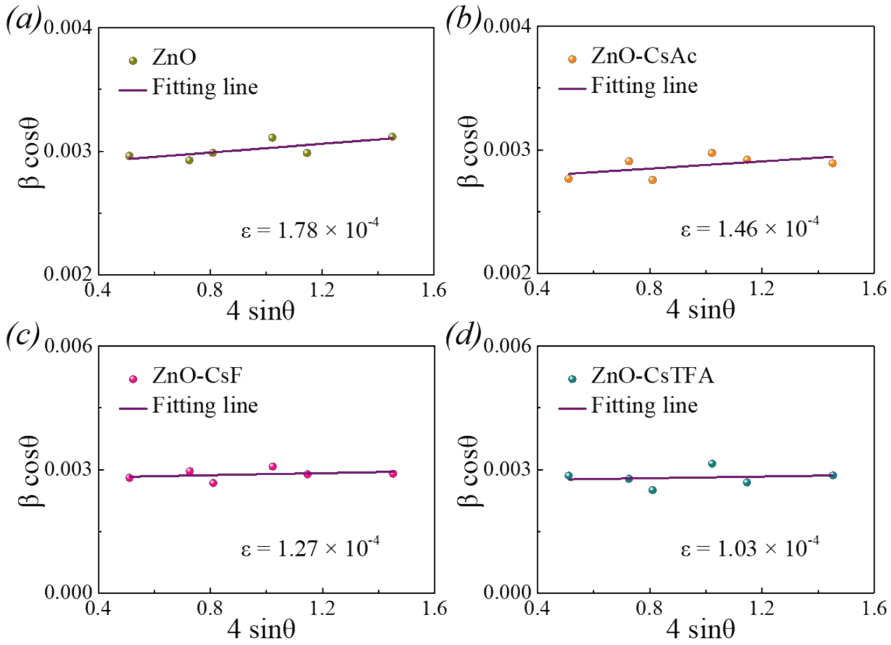

Fig. S29 Williamson-Hall plots of $CsPbI_2Br$ films on the (a) ZnO, (b) ZnO-CsAc, (c) ZnO-CsF, and (d) ZnO-CsTFA ETLs.

The residual strain of $CsPbI_2Br$ films can be evaluated from the XRD patterns (Fig. 4i) by Williamson-Hall analysis:[8, 9]

$$\beta cos\theta = \varepsilon(4sin\theta) + \frac{k\lambda}{D} \qquad \text{Equation S2}$$

where β is the FWHM of XRD peak, θ is the diffraction angle, ε is the residual strain (the slope of fitted line), k is the shape factor that is 0.9 for a cubic structure, λ is the wavelength of X-ray source, and D is the crystallite size.

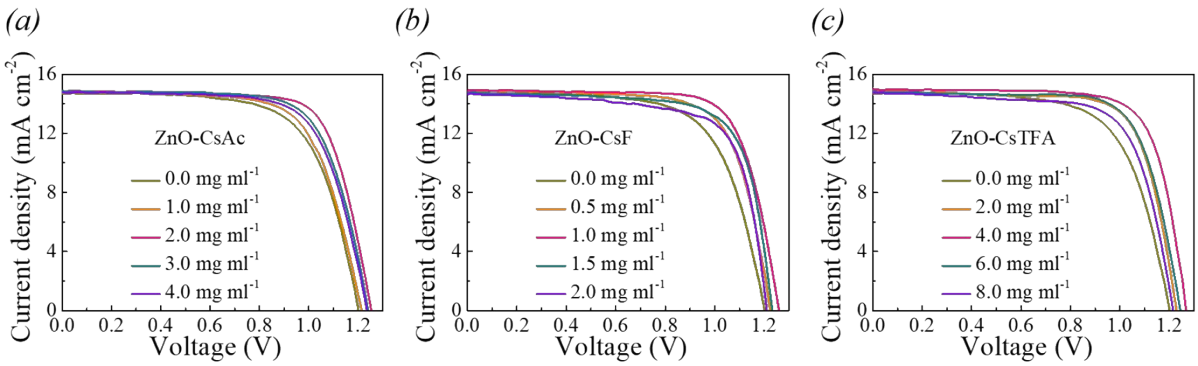

Fig. S30 J-V curves for C-IPSCs modified with different cesium modulators concentration.

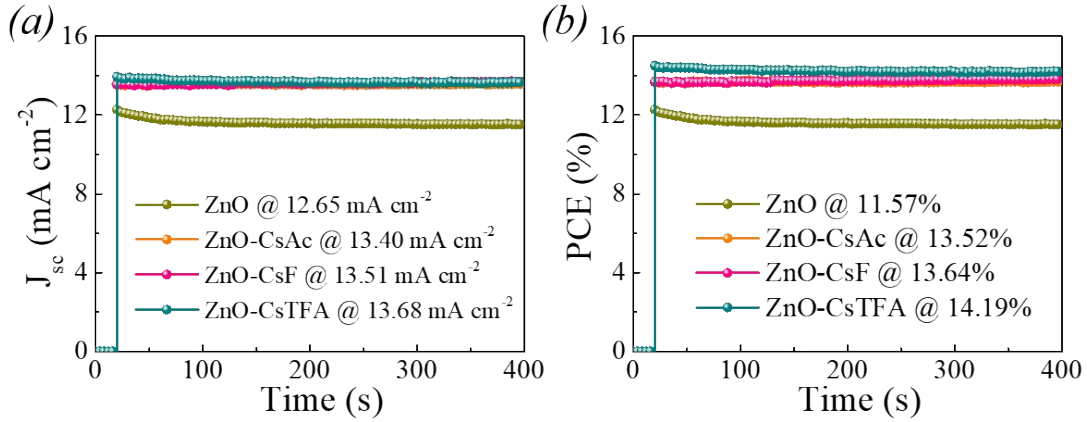

Fig. S31 Steady-state (a) J_{sc} and (b) PCE profile at the maximum power point.

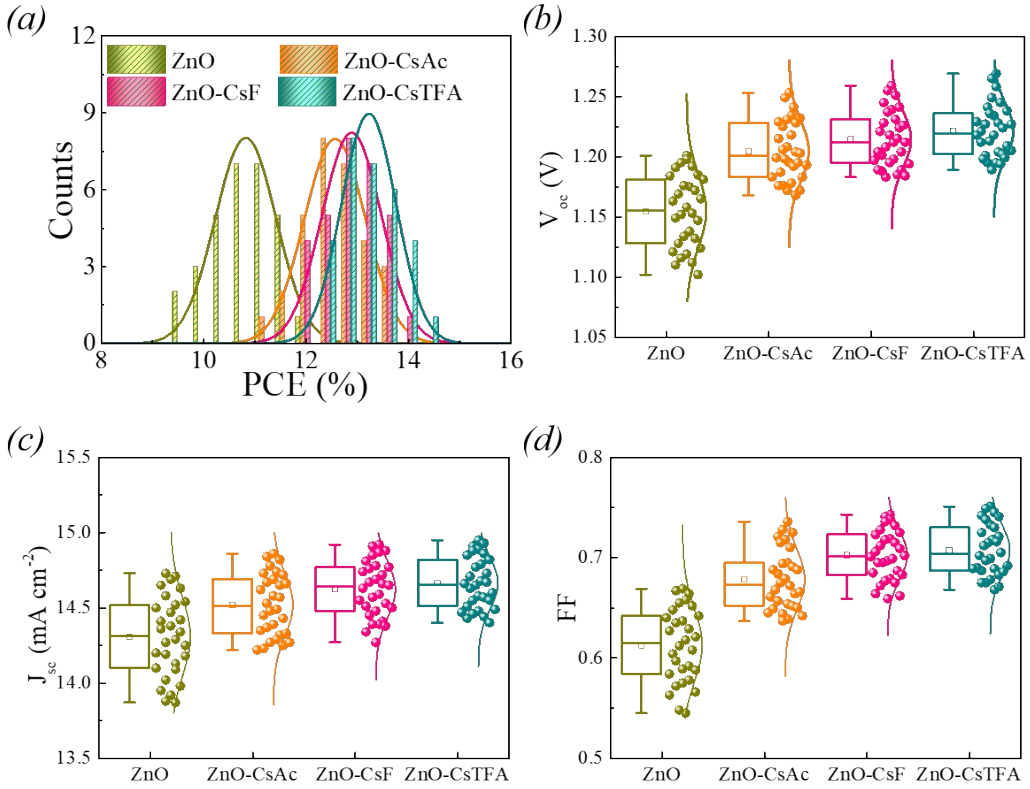

Fig. S32 (a) PCE, (b) V_{oc}, (c) J_{sc}, and (d) FF distributions from 30 individual devices.

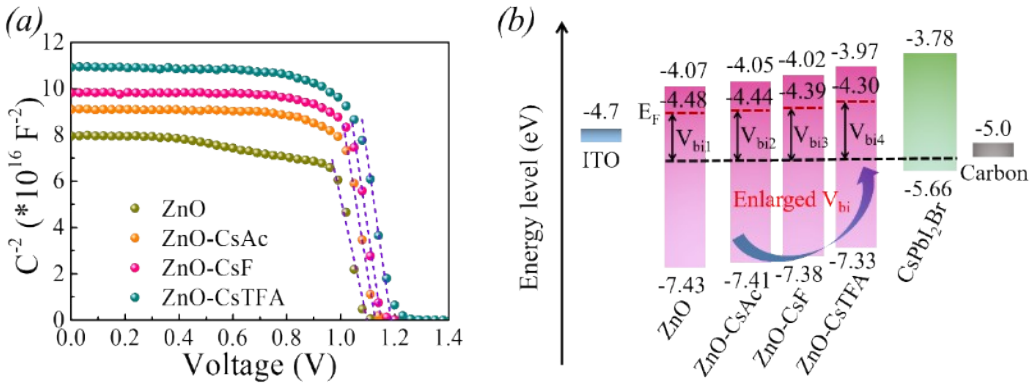

Fig. S33 (a) C^{-2}-V plots of C-IPSCs. (b) Schematic illustration of the built-in potential (V_{bi}) behavior of C-IPSCs based on the pristine and doped ZnO ETLs.

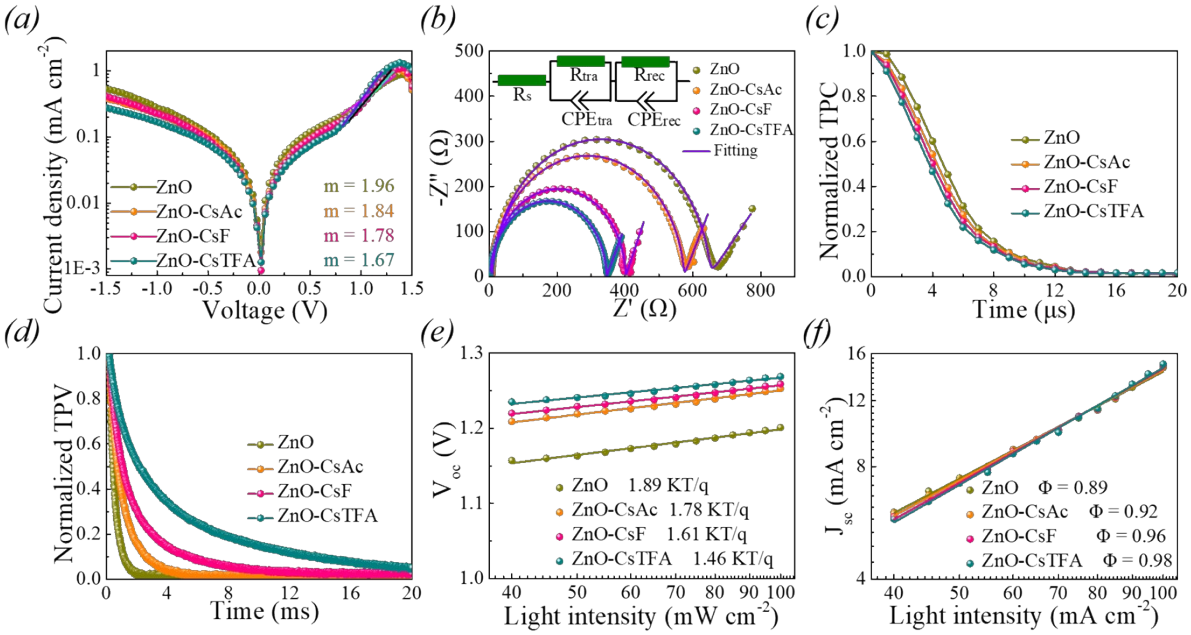

Fig. S34 (a) Dark J-V curves of C-IPSCs. (b) Nyquist plots under illumination condition at 1.2 V. Inset: equivalent circuit model. (c) Normalized TPC and (d) TPV decay curves of C-IPSCs. (e) V_{oc} and (f) J_{sc} dependence on different P_{light} of C-IPSCs.

The ideally factor (m) of dark J-V curve is obtained by the Equation S3:[10]

$$m = \frac{KT}{q}\frac{dlnJ}{dV} \qquad \text{Equation S3}$$

The V_{oc} versus P_{light} relationship is fitted by the Equation S4:[11]

$$V_{oc} = \frac{nKT}{q}\ln\left(P_{light}\right) + constant \qquad \text{Equation S4}$$

The J_{sc} versus P_{light} relationship is fitted by a power-law equation:[11]

$$J_{sc} \propto P_{light}^{\Phi} \qquad \Phi \leq 1 \qquad \text{Equation S5}$$

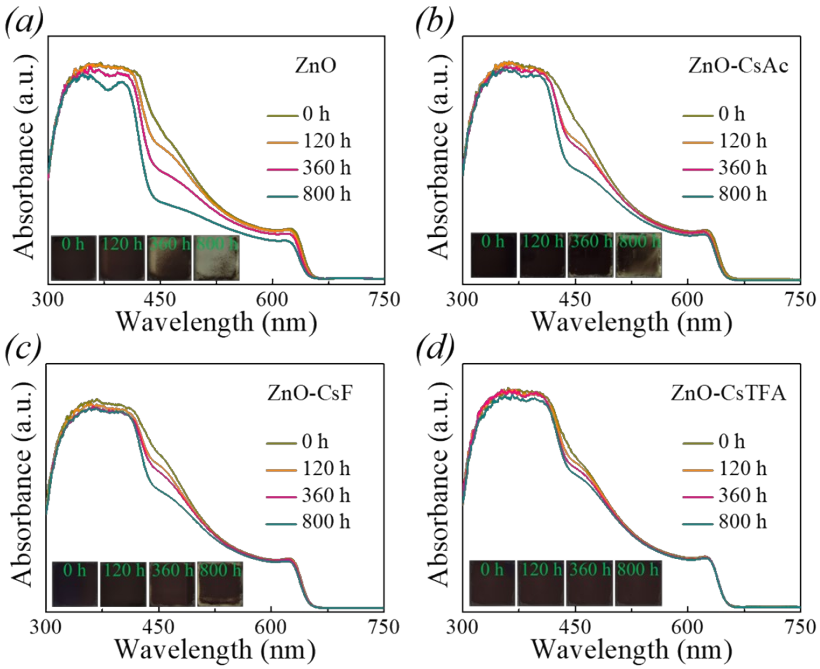

Fig. S35 Temporal evolution of UV-vis absorption spectra for moisture-aged $CsPbI_2Br$ films on the (a) ZnO, (b) ZnO-CsAc, (c) ZnO-CsF, and (d) ZnO-CsTFA ETLs. Inset: photographs of morphology changes for $CsPbI_2Br$ films.

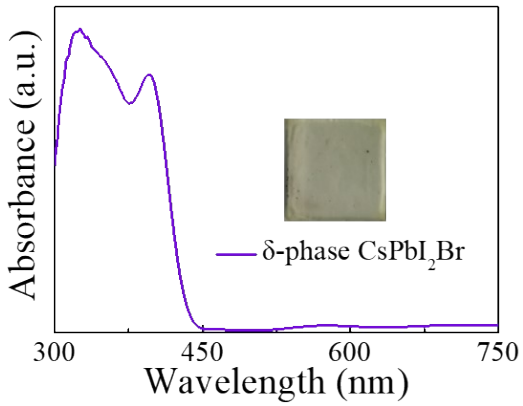

Fig. S36 UV-vis absorption spectra of δ-phase $CsPbI_2Br$ films. Innet: corresponding photograph.

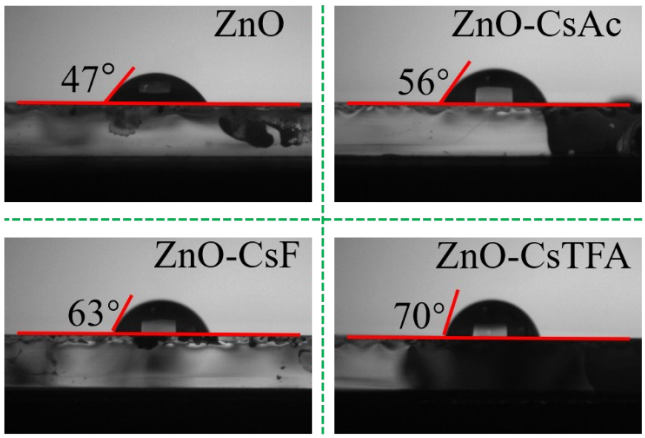

Fig. S37 Water contact angles of $CsPbI_2Br$ films on the pristine and doped ZnO ETLs.

Table Section

Table S1 Position, area (S), and S ratio of deconvoluted O 1s peaks for pristine and doped ZnO ETLs.

O 1s		ZnO	ZnO-CsAc	ZnO-CsF	ZnO-CsTFA
O_L	Position (eV)	529.79	529.94	529.90	530.15
	S_L	56219.48	71382.2	92583.1	99929.0
O_V	Position (eV)	531.17	531.19	531.00	531.34
	S_V	30216.9	34819.2	32017.2	20840.2
O_{OH}	Position (eV)	532.16	532.24	531.88	532.07
	S_{OH}	10626.6	11592.7	18130.1	12000.0
S ratio	$S_L/(S_L + S_V + S_{OH})$	0.58	0.61	0.65	0.75
	$S_V/(S_L + S_V + S_{OH})$	0.31	0.29	0.22	0.16
	$S_{OH}/(S_L + S_V + S_{OH})$	0.11	0.10	0.13	0.09
	$S_V+S_{OH}/(S_L + S_V + S_{OH})$	0.42	0.39	0.35	0.25

Table S2 The calculated σ values of pristine and doped ZnO ETLs.

ETL	Slop [I/V]	Device area (cm^2)	Thickness (nm)	σ ($mS\ cm^{-1}$)
ZnO	50.18	0.09	40	2.23×10^{-3}
ZnO-CsAc	61.41	0.09	40	2.73×10^{-3}
ZnO-CsF	66.83	0.09	40	2.97×10^{-3}
ZnO-CsTFA	71.38	0.09	40	3.17×10^{-3}

The σ values of pristine and doped ZnO ETLs are calculated from the slopes (I/V) of dark current-voltage (I-V) curves according to the Equation S6:[12]

$$\sigma = \frac{Id}{VA} \qquad \text{Equation S6}$$

where A represents the device area (0.09 cm^2).

Table S3 The calculated μ_e values of pristine and doped ZnO ETLs.

ETL	Thickness (nm)	μ_e (cm^{-2} V^{-1} s^{-1})
ZnO	40	6.57×10^{-3}
ZnO-CsAc	40	6.86×10^{-3}
ZnO-CsF	40	7.07×10^{-3}
ZnO-CsTFA	40	7.15×10^{-3}

The SCLC model is applied to electron-only device (glass/ITO/Ag/pristine or doped ZnO/Ag) to estimate the μ_e values of pristine and doped ZnO ETLs, as follows:[11]

$$\mu_e = \frac{8Jd^3}{9\varepsilon_0\varepsilon_i V^2} \quad \text{Equation S7}$$

Table S4 Relative normalized peak intensity and FWHM of pristine and doped ZnO ETLs.

ETL	(100) relative normalized peak intensity	FWHM of (100) (degree)	(110) relative normalized peak intensity	FWHM of (110) (degree)
ZnO	0.70	0.52	0.65	0.53
ZnO-CsAc	0.87	0.49	0.77	0.46
ZnO-CsF	0.91	0.41	0.82	0.42
ZnO-CsTFA	1.00	0.39	1.00	0.31

Table S5 Detailed parameters derived from the UPS spectra for pristine and ZnO ETLs.

ETL	E_{onset} (eV)	E_{offset} (eV)	VBM (eV)	CBM (eV)	E_F (eV)	W_F (eV)	E_g (eV)
ZnO	2.95	16.74	-7.43	-4.07	-4.48	4.48	3.36
ZnO-CsAc	2.97	16.78	-7.41	-4.05	-4.44	4.44	3.36
ZnO-CsF	2.99	16.83	-7.38	-4.02	-4.39	4.39	3.36
ZnO-CsTFA	3.03	16.92	-7.33	-3.97	-4.30	4.30	3.36

The work function (W_F) and Fermi level (E_F) values of pristine and doped ZnO ETLs are estimated according to the following Equations S8 and S9:[13]

$$W_F = E_{cutoff} - 21.22 \quad \text{Equation S8}$$

$$E_F = -W_F \quad \text{Equation S9}$$

The valence band maximum (VBM) and conduction band minimum (CBM) values are calculated by the following Equations S10 and S11:[11]

$$VBM = E_{offset} - E_{onset} - 21.22 \quad \text{Equation S10}$$

$$CBM = VBM + E_g \quad \text{Equation S11}$$

Table S6 Relative normalized peak intensity and FWHM of $CsPbI_2Br$ films on the pristine and doped ZnO ETLs.

$CsPbI_2Br$	(100) relative normalized peak intensity	FWHM of (100) (degree)	(200) relative normalized peak intensity	FWHM of (200) (degree)
ZnO	0.55	0.171	0.57	0.226
ZnO-CsAc	0.74	0.163	0.78	0.218
ZnO-CsF	0.84	0.159	0.89	0.209
ZnO-CsTFA	1.00	0.155	1.00	0.203

Table S7 Fitting parameters of TRPL decay spectra based on the glass/ITO/ZnO/$CsPbI_2Br$, glass/ITO/ZnO-CsAc/$CsPbI_2Br$, glass/ITO/ZnO-CsF/$CsPbI_2Br$, and glass/ITO/ZnO-CsTFA/$CsPbI_2Br$ samples.

Sample	A_1	τ_1 (ns)	τ_1 (%)	A_2	τ_2 (ns)	τ_2 (%)	τ_{pl} (ns)
glass/ITO/ZnO/$CsPbI_2Br$	0.80	9.97	94.99	0.16	2.63	5.01	9.60
glass/ITO/ZnO-CsAc/$CsPbI_2Br$	0.82	8.30	98.55	0.10	1.00	1.45	8.19
glass/ITO/ZnO-CsF/$CsPbI_2Br$	0.83	6.11	97.11	0.18	0.84	2.89	5.96
glass/ITO/ZnO-CsTFA/$CsPbI_2Br$	0.85	4.33	96.31	0.17	0.83	3.69	4.20

The TRPL decay spectrum is fitted by the bi-exponential function (Equation S12):[11]

$$y(t) = A_1 e^{-t/\tau_1} + A_2 e^{-t/\tau_2} + y_0 \quad \text{Equation S12}$$

where A_1 and A_2 represent weighting coefficients of each decay channel, τ_1 and τ_2 are first- and second-order decay times, y_0 is a constant.

The average PL lifetime (τ_{pl}) of TRPL decay spectra can be calculated by the following Equation S13:[11]

$$\tau_{pl} = \frac{A_1\tau_1}{A_1\tau_1 + A_2\tau_2}\tau_1 + \frac{A_2\tau_2}{A_1\tau_1 + A_2\tau_2}\tau_2 \quad \text{Equation S13}$$

Table S8 Fitting parameters of TA spectra based on the glass/ITO/ZnO/$CsPbI_2Br$, glass/ITO/ZnO-CsAc/$CsPbI_2Br$, glass/ITO/ZnO-CsF/$CsPbI_2Br$, and glass/ITO/ZnO-CsTFA/$CsPbI_2Br$ samples.

Sample	A_1	τ_1 (ps)	τ_1 (%)	A_2	τ_2 (ps)	τ_1 (%)	τ_{ta} (ps)
glass/ITO/ZnO/$CsPbI_2Br$	0.19	3243.70	94.18	0.15	253.87	5.82	3069.71
glass/ITO/ZnO-CsAc/$CsPbI_2Br$	0.24	2931.07	97.58	0.14	124.44	2.42	2863.24
glass/ITO/ZnO-CsF/$CsPbI_2Br$	0.23	2873.22	93.11	0.17	287.90	6.89	2694.95
glass/ITO/ZnO-CsTFA/$CsPbI_2Br$	0.12	1876.59	92.17	0.14	136.73	7.83	1740.28

The kinetic decay trace of PB negative peak is fitted by the Equation S12. The average TA lifetime (τ_{ta}) is calculated by the Equation S13.

Table S9 The calculated N_t values of $CsPbI_2Br$ films on the pristine and doped ZnO ETLs.

Device	ZnO	ZnO-CsAc	ZnO-CsF	ZnO-CsTFA
V_{TFL} (V)	1.045	1.015	0.994	0.899
N_t (10^{15} cm^{-3})	5.639	5.477	5.363	4.851

The SCLC model was applied to electron-only device (glass/ITO/pristine or doped ZnO/$CsPbI_2Br$/$PC_{61}BM$/Ag) to quantitatively estimate the trap state density (N_t) values of perovskite fims. The relative permittivity of $CsPbI_2Br$ is 8.5.[7] The trap-filled limit voltage (V_{TFL}) is the voltage at the kink point.

Table S10 Photovoltaic parameters of C-IPSCs based on the CsAc-modulated ZnO ETLs prepared with different CsAc concentrations.

Concentration (mg ml^{-1})	V_{oc} (V)	J_{sc} (mA cm^{-2})	FF	PCE (%)
0.0	1.201	14.71	0.669	11.82
1.0	1.219	14.81	0.682	12.31
2.0	1.253	14.86	0.736	13.70
3.0	1.240	14.84	0.712	13.10
4.0	1.235	14.75	0.701	12.77

Table S11 Photovoltaic parameters of C-IPSCs based on the CsF-modulated ZnO ETLs prepared with different CsF concentrations.

Concentration (mg ml^{-1})	V_{oc} (V)	J_{sc} (mA cm^{-2})	FF	PCE (%)
0.0	1.201	14.71	0.669	11.82
0.5	1.224	14.86	0.717	13.04
1.0	1.259	14.92	0.743	13.96
1.5	1.233	14.78	0.728	13.27
2.0	1.211	14.68	0.715	12.71

Table S12 Photovoltaic parameters of C-IPSCs based on the CsTFA-modulated ZnO ETLs prepared with different CsTFA concentrations.

Concentration (mg ml^{-1})	V_{oc} (V)	J_{sc} (mA cm^{-2})	FF	PCE (%)
0.0	1.201	14.71	0.669	11.82
2.0	1.230	14.87	0.736	13.46
4.0	1.269	14.95	0.751	14.25
6.0	1.245	14.81	0.734	13.53
8.0	1.216	14.73	0.707	12.66

Table S13 Photovoltaic parameters of C-IPSCs in both the reverse scan (RS) and forward scan (FS) directions. The hysteresis index (HI) is defined as: $HI = (PCE_{RS} - PCE_{FS})/PCE_{RS}$.

Device	Scan direction	V_{oc} (V)	J_{sc} (mA cm^{-2})	FF	PCE (%)	HI
ZnO	RS	1.201	14.71	0.669	11.82	0.107
	FS	1.187	14.69	0.605	10.55	
ZnO-CsAc	RS	1.253	14.86	0.736	13.70	0.056
	FS	1.244	14.83	0.701	12.93	
ZnO-CsF	RS	1.259	14.92	0.743	13.96	0.018
	FS	1.250	14.92	0.735	13.71	
ZnO-CsTFA	RS	1.269	14.95	0.751	14.25	0.050
	FS	1.266	14.94	0.716	13.54	

Table S14 Photovoltaic performance comparisons of ZnO-based C-IPSCs reported so far.

No.	Perovskite	Device structure	V_{oc} (V)	J_{sc} (mA cm^{-2})	FF	PCE (%)	Year	Ref.
1	$CsPbI_2Br$	glass/ITO/ZnO-CsTFA/$CsPbI_2Br$/carbon	1.269	14.95	0.751	14.25	2023	This work
2	$CsPbIBr_2$	glass/FTO/ZnO/$CsPbIBr_2$/carbon	1.09	13.74	0.56	8.42	2021	14
3	$CsPbI_{3-x}Br_x$	glass/FTO/DI H_2O/ZnO/$CsPbI_{3-x}Br_x$/carbon	0.96	19.10	0.68	12.39	2022	15
4	$CsPbI_3$	glass/FTO/ZnO/$CsPbI_3$/carbon	0.91	17.66	0.68	10.95	2020	16
5	$CsPbIBr_2$	glass/FTO/ZnO/$CsPbIBr_2$/carbon	1.03	11.60	0.63	7.60	2019	17
6	$CsPbIBr_2$	glass/FTO/(Ag)ZnO/$CsPbIBr_2$/carbon	0.8	8.02	0.42	2.70	2022	18

Table S15 The steady-state J_{sc} and PCE values derived from the stabilized power output curves for pristine and doped ZnO ETLs.

Device	Maximum power point V_{oc} (V)	Steady-state J_{sc} (mA cm^{-2})	Steady-state PCE (%)
ZnO	0.915	12.65	11.57
ZnO-CsAc	1.009	13.40	13.52
ZnO-CsF	1.010	13.51	13.64
ZnO-CsTFA	1.037	13.68	14.19

Table S16 The V_{bi} values obtained from C^{-2}-V plots.

Device	ZnO	ZnO-CsAc	ZnO-CsF	ZnO-CsTFA
V_{bi} (V)	1.098	1.127	1.151	1.187

The V_{bi} values were extracted based on Mott-Schottky analysis, and the relevant equation is as follows:[19]

$$C^{-2} = \frac{2(V_{bi} - V)}{A^2 \varepsilon_0 \varepsilon_r q N_A} \quad \text{Equation S14}$$

where N_A is the carrier concentration.

Table S17 Fitting parameters obtained from the Nyquist plots of C-IPSCs measured at a bias of 1.20 V under illumination.

Device	R_s ($\Omega \cdot cm^2$)	R_{tra} ($\Omega \cdot cm^2$)	CPE_{tra}-T (nF cm^{-2})	CPE_{tra}-P	R_{rec} ($\times 10^4$ $\Omega \cdot cm^2$)	CPE_{rec}-T ($\times 10^7$ nF cm^{-2})	CPE_{rec}-P
ZnO	0.78	57.49	387.82	0.97	8.80	2.23	0.54
ZnO-CsAc	0.63	50.97	397.56	0.97	10.17	1.98	0.70
ZnO-CsF	0.40	35.79	155.89	0.99	12.17	2.16	0.74
ZnO-CsTFA	0.28	30.84	152.89	0.99	14.21	2.84	0.71

Table S18 Fitting parameters of normalized TPC decay curves.

Device	ZnO	ZnO-CsAc	ZnO-CsF	ZnO-CsTFA
τ_{tra} (μs)	5.66	5.16	4.83	4.50

The charge transport time (τ_{tra}) is obtained from normalized TPC data fitted by a single-exponential function:[11]

$$y(t) = A_3 e^{-t/\tau_{tra}} + y_0 \qquad \text{Equation S15}$$

Table S19 Fitting parameters of normalized TPV decay curves.

Device	A_1	τ_1 (ms)	τ_1 (%)	A_2	τ_2 (ms)	τ_2 (%)	τ_{rec} (ms)
ZnO	0.73	0.49	50.00	0.73	0.49	50.00	0.49
ZnO-CsAc	0.95	0.92	82.70	0.04	4.57	17.30	1.55
ZnO-CsF	0.68	3.44	66.05	0.35	0.91	33.95	2.58
ZnO-CsTFA	0.48	7.99	82.27	0.57	1.45	17.73	6.83

The normalized TPV data are fitted by the Equation S12. The charge recombination lifetime (τ_{rec}) is calculated by the Equation S13.

References

1 M. J. Frisch, G. W. Trucks, H. B. Schlegel, G. E. Scuseria, M. A. Robb, J. R. Cheeseman, G. Scalmani, V. Barone, G. A. Petersson, H. Nakatsuji, X. Li, M. Caricato, A. V. Marenich, J. Bloino, B. G. Janesko, R. Gomperts, B. Mennucci, H. P. Hratchian, J. V. Ortiz, A. F. Izmaylov, J. L. Sonnenberg, Williams, F. Ding, F. Lipparini, F. Egidi, J. Goings, B. Peng,

A. Petrone, T. Henderson, D. Ranasinghe, V. G. Zakrzewski, J. Gao, N. Rega, G. Zheng, W. Liang, M. Hada, M. Ehara, K. Toyota, R. Fukuda, J. Hasegawa, M. Ishida, T. Nakajima, Y. Honda, O. Kitao, H. Nakai, T. Vreven, K. Throssell, J. A. Montgomery Jr., J. E. Peralta, F. Ogliaro, M. J. Bearpark, J. J. Heyd, E. N. Brothers, K. N. Kudin, V. N. Staroverov, T. A. Keith, R. Kobayashi, J. Normand, K. Raghavachari, A. P. Rendell, J. C. Burant, S. S. Iyengar, J. Tomasi, M. Cossi, J. M. Millam, M. Klene, C. Adamo, R. Cammi, J. W. Ochterski, R. L. Martin, K. Morokuma, O. Farkas, J. B. Foresman and D. J. Fox, *Wallingford, CT*, 2016.

2 C. Adamo and V. Barone, *J. Chem. Phys.*, 1999, **110**, 6158-6170.

3 D. Andrae, U. Häußermann, M. Dolg, H. Stoll and H. Preuß, *Theor. Chim. Acta*, 1990, **77**, 123-141.

4 R. Krishnan, J. S. Binkley, R. Seeger and J. A. Pople, *J. Chem. Phys.*, 1980, **72**, 650-654.

5 S. Grimme, S. Ehrlich and L. Goerigk, *J. Comput. Chem.*, 2011, **32**, 1456-1465.

6 G. Scalmani and M. J. Frisch, *J. Chem. Phys.*, 2010, **132**, 114110.

7 X. Zhang, N. Gao, Y. Li, L. Xie, X. Yu, X. Lu, X. Gao, J. Gao, L. Shui, S. Wu and J.-M. Liu, *ACS Appl. Energy Mater.*, 2020, **3**, 7832-7843.

8 H. Cheng, C. Liu, J. Zhuang, J. Cao, T. Wang, W.-Y. Wong and F. Yan, *Adv. Funct. Mater.*, 2022, **32**, 2204880.

9 Z. Zheng, F. Li, J. Gong, Y. Ma, J. Gu, X. Liu, S. Chen and M. Liu, *Adv. Mater.*, 2022, **34**, 2109879.

10 S. Xiong, Z. Hou, S. Zou, X. Lu, J. Yang, T. Hao, Z. Zhou, J. Xu, Y. Zeng, W. Xiao, W. Dong, D. Li, X. Wang, Z. Hu, L. Sun, Y. Wu, X. Liu, L. Ding, Z. Sun, M. Fahlman and Q. Bao, *Joule*, 2021, **5**, 467-480.

11 X. Zhang, D. Zhang, Y. Zhou, Y. Du, J. Jin, Z. Zhu, Z. Wang, X. Cui, J. Li, S. Wu, J. Zhang and Q. Tai, *Adv. Funct. Mater.*, 2022, **32**, 2205478.

12 S. Yang, W. Liu, Y. Han, Z. Liu, W. Zhao, C. Duan, Y. Che, H. Gu, Y. Li and S. Liu, *Adv. Energy Mater.*, 2020, **10**, 2002882.

13 T. Wu, R. Zhao, J. Qiu, S. Wang, X. Zhang and Y. Hua, *Adv. Funct. Mater.*, 2022, **32**, 2204450.

14 L. Gong, J.-S. Zhang, C. Wang, H. Fu, Y.-F. Lu, J.-L. Chen, J.-C. Fan and Z.-S. Chao, *ACS Appl. Energy Mater.*, 2021, **4**, 4686-4694.

15 H. Fu, J. Zhang, Y. Li, L. Gong, H. He, Z. Fang, C. Zhou, J. Chen and J. Fan, *J. Mater. Sci.: Mater. Electron.*, 2022, **33**, 3711-3725.

16 J. Zhang, C. Wang, H. Fu, L. Gong, H. He, Z. Fang, C. Zhou, J. Chen, Z. Chao and J. Fan,

J. Alloys Compd., 2021, **862**, 158454.

17 C. Wang, J. Zhang, L. Jiang, L. Gong, H. Xie, Y. Gao, H. He, Z. Fang, J. Fan and Z. Chao, *J. Alloys Compd.*, 2020, **817**, 152768.

18 Y. Huang, Y. Wu, X. Xu, F. Qin, S. Zhang, J. An, H. Wang and L. Liu, *Chinese Phys. B*, 2022, **31**, 128802.

19 Y. Ge, F. Ye, M. Xiao, H. Wang, C. Wang, J. Liang, X. Hu, H. Guan, H. Cui, W. Ke, C. Tao and G. Fang, *Adv. Energy Mater.*, 2022, **12**, 2200361.